Journal of Porous Materials (2021) 28:261–269
https://doi.org/10.1007/s10934-020-00988-9

Functionalized hierarchical wrinkled-silica spheres for laccases immobilization

Keyla M. Fuentes[1] · Lucy L. Coria-Oriundo[2,3] · Sonia Wirth[4] · Sara A. Bilmes[2,3]

Accepted: 18 September 2020 / Published online: 22 September 2020

Abstract

Functionalized mesoporous SiO_2 are common supports for some enzymes of industrial interest, such as laccases. However, the incorporation of specific functionalities and the loading of enzymes with dimensions close to the diameters of the pores obstructs the porous system. For biotechnological applications, tailored porous supports are still needed to enhance the laccase loading. The hierarchical meso/macroporous system in wrinkled-SiO_2 spheres (w-SiO_2) is a suitable option to overcome this issue. Herein, (3-aminopropyl) triethoxysilane and glutaraldehyde were use as functionalizing agents for the immobilization of laccase on w-SiO_2. The functionalization occurs in the mesopores of the wrinkled walls and the preservation of the macroporous entries facilitates the diffusion of the laccase inside the particle. The enzyme performance was evaluated by means of the crystal violet bleaching. The enzyme is stabilized through the imine groups provided by glutaraldehyde, allowing the retention of the activity after several reaction cycles. The bleaching can be boosted by acetosyringone, highlighting the possibility of using redox mediators to expand the range of oxidizable substrates. Understanding the effect of w-SiO_2 functionalization on laccases loading and performance could be extrapolated to other enzymes with biotechnological interest that requires this type of hierarchical porous silica.

Keywords Hierarchical porous silica · Silica functionalization · Enzyme immobilization

1 Introduction

Enzymes immobilization onto mesoporous SiO_2 is a common strategy for the implementation of biotechnological processes at industrial level mainly due to the thermal and mechanical stability and large surface areas of these materials [1–4]. However, two main challenges arise for an effective enzyme immobilization: (*i*) low retention of the enzyme due to a weak enzyme-support interaction, and (*ii*) as the particle is loaded, the clogging of the porous system causes a decrease in the availability of surface sites limiting the amount of immobilized enzyme. A strong enzyme-support interaction can be addressed to a covalent binding with specific amino acids in the enzyme [5]. Some functional groups can be incorporated into the SiO_2 surface mainly through post-synthesis protocols, such as grafting [6]. Unfortunately, the functionalization is usually accompanied by a drastic reduction in the textural characteristics of the material since grafting occurs mainly in the mesopores [7]. Therefore, a model support should possess a pore size distribution such that it provides elevated surface areas for high loadings and

Electronic supplementary material The online version of this article (https://doi.org/10.1007/s10934-020-00988-9) contains supplementary material, which is available to authorized users.

✉ Keyla M. Fuentes
keyla.fuentes@cimav.edu.mx

✉ Sara A. Bilmes
sarabil@qi.fcen.uba.ar

[1] Centro de Investigación en Materiales Avanzados, S. C. (CIMAV), Unidad Monterrey, Parque de Investigación e Innovación Tecnológica, Alianza Norte 202, 66628 Apodaca, Nuevo León, México

[2] CONICET – Universidad de Buenos Aires, Instituto de Química Física de los Materiales, Medio Ambiente y Energía- INQUIMAE, Pza. Gregorio Klimovsky, Ciudad Universitaria, Universidad de Buenos Aires, Pabellón 2, C1428EHA Ciudad de Buenos Aires, Argentina

[3] Departamento de Química Inorgánica, Analítica y Química Física, DQIAQF, Universidad de Buenos Aires, Facultad de Ciencias Exactas y Naturales, FCEyN, Ciudad de Buenos Aires, Argentina

[4] Laboratorio de Agrobiotecnología, DFBMC-FCEN-UBA and IBBEA, CONICET-UBA, C1428EGA, Ciudad de Buenos Aires, Argentina

enough space to lodge the enzyme without clogging the porous system.

In this regard, the unique configuration of the hierarchical meso/macroporous system in wrinkled SiO_2 spheres is suitable for enzyme immobilization because of it provides high surface area and pores volume, as well as pores diameters larger than the dimensions of several enzymes [8]. Some examples of enzymes physically immobilized in this type of hierarchical silica have been recently reported for different applications. For instance, catalase has been immobilized with high loadings showing an enhanced activity for H_2O_2 decomposition [9]. Physically immobilized lipase and β-glucosidase have also revealed potential for biofuel production [10, 11]. Despite the advantages associated with the *w*-SiO_2 morphology to obtain high enzyme loadings, the functionalization effect on the porous system is not clear, nor how this could affect the enzymes performance.

Laccases (benzenediol: oxygen oxidoreductase, EC 1.10.3.2) have significant industrial interest due to their ability to oxidize a wide variety of phenolic and amino-aromatic compounds, being useful in several industrial fields; such as, paper, textile, food processing and bioremediation [12–14]. The application of recombinant expression systems allows the improvement in the production and the design some enzymatic features for specific needs [15–17]. For instance, the recombinant LCC3 from *Trametes trogii* possesses a 6-histidine fusion that could favor the immobilization. As a free enzyme, it showed high activity at temperatures above 50 °C with retention of the activity at pH = 6 during the degradation of several dyes, and it has been used as electrochemical sensor for phenol-like compounds [18, 19].

According to the above, the immobilization of LCC3 on functionalized *w*-SiO_2 is a promising strategy to obtain an efficient biocatalyst, taking advantage of the meso/macroporous system to allow high enzyme loading, with retained activity and reusability. In this work, *w*-siO_2 was functionalized with (3-aminopropyl) triethoxysilane and glutaraldehyde to evaluate the effect of functionalization on the enzyme loading and performance. The loading capacity of the material was compared to known systems, while the performance of the biocatalyst was tested for crystal violet bleaching under several reaction conditions.

2 Experimental

2.1 Materials

Tetraethyl orthosilicate (TEOS) 98%, (3-Aminopropyl) triethoxysilane (APTES) 99%, urea 99%, hexadecyltrimethylammonium bromide (CTAB) 95%, Laccase LcTv (*Trametes versicolor)* and 2,2′-azino-bis (3-ethylbenzothiazoline-6-sulfonic acid) (ABTS) were purchased from Sigma-Aldrich (USA). Cyclohexane, ethanol, 1-butanol, 2-propanol, and acetone were acquired from Sintorgan (Argentina). Citrate–phosphate buffers (McIlvane's buffer) were prepared with citric acid and potassium phosphate monobasic acquired from Merck. All chemicals were used without further purification. Milli-Q water (18 MΩ) was employed for preparing all the solutions.

2.2 Synthesis of *w*-SiO_2 host

Silica mesostructures were prepared based on the pseudo-ternary system proposed by Moon and Lee [20]. For this method the aqueous phase is a 0.4 M urea solution; a mixture of CTAB and 1-butanol (1:1 w/w) acts as the surfactant component, and the oil phase is cyclohexane. For a typical synthesis of porous spheres *c.a.*, 0.5 µm in diameter: 0.5 g of CTAB and 0.5 g of 1-butanol were dissolved on 7.5 g of urea solution using a glass vial of 25 mL. Then, 7.5 g of cyclohexane was added to the mixture and the glass vial was tightly closed using a septum and a metal seal. The mixture was left under vigorous stirring (900 rpm) at 25 °C for 5 min. After this time, 0.54 mL of TEOS was added dropwise to the emulsion using a syringe and left under stirring for 30 min at room temperature. The reaction mixture was then heated at 70 °C during 19 h. The particles were collected at the interface after the addition of acetone and centrifugation at 3000 rpm for 5 min. To remove the remaining template, the solid was suspended on a 6 wt.% NH_4NO_3/ethanol solution for 12 h at 70 °C, this process was repeated until the fading of the -CH_2, -CH_3 vibration modes in the FT-IR spectrum, corresponding to the CTAB molecules. Finally, the samples were washed with deionized water, centrifuged and dried at 70 °C. This solid is named *w*-SiO_2.

2.3 *w*-SiO_2 functionalization

The amino moieties were incorporated by grafting procedure. For this, 0.2 g of *w*-SiO_2 was dispersed in 20 mL of dry toluene, then 2 mL of APTES were added and the mixture was refluxed at 80 °C for 24 h. The suspension was filtered, washed twice with dry toluene and three times with acetone; the solid was dried under vacuum. This material is labelled *w*-SiO_2-NH_2. Then, a portion of the amino-functionalized support was modified by adding glutaraldehyde as cross-linker. In this step, 0.1 g of the *w*-SiO_2-NH_2 spheres were suspended in 20 mL of glutaraldehyde solution (4 w/v %) prepared in PBS 1X (pH = 7.4). The mixture was stirred during 8 h at 25 °C. The solid was centrifuged and washed thrice with PBS solution to remove any glutaraldehyde not covalently bonded. The solid was washed three times with acetone and finally dried under vacuum. This solid is named *w*-SiO_2-NH_2-GA.

2.4 Characterization

The particles morphology was evaluated with scanning electron microscopy (SEM), the images were obtained using a Field Emission Gun Scanning Electron Microscope (FEG-SEM) (Zeiss Supra 40). The accelerating voltage for the electronic beam was 3 KV. For this analysis the samples were sonicated 10 min in ethanol and, a drop of the solution was deposited in a silicon plate. For TEM analysis the suspension was dropped on a carbon-coated copper grid (CFC-200 Cu, EMS, USA), the images were taken using a JEM-2100 transmission electron microscope JEOL, equipped with a LaB_6 anode operating at an accelerating voltage of 200 kV. TGA analysis was conducted in a TGA-51H thermogravimetric analyzer from Shimadzu. The samples were heated up to 800 °C with a ramp rate of 10 °C/min under a 30 mL/min N_2 flow. KBr pellets were prepared to measure the FTIR spectra using a Nicolet 8700 Spectrometer equipped with a DTGS detector. The spectral range was evaluated in the 4000- 400 cm^{-1} region; the resolution was 4 cm^{-1} by collecting 32 scans.

Nitrogen content was quantified through elemental analysis (CHN) using a combustion reactor Carlo Erba EA 1108; the oxidation products were separated in a porapac column and measured with a thermal conductivity detector using gas chromatography. Sulfanilic acid was used as calibration control. Surface area and pore size distribution were analyzed using N_2 adsorption–desorption isotherms at 77 K using an Accelerated Surface Area and Porosimetry System (ASP 2420) from Micromeritics. The surface area was calculated by the B.E.T. method, and the BJH model to calculate the pore size distribution.

2.5 Laccase activity essay

The activity of free laccase (initial and final) was determined by UV–Vis spectrometry, measuring the absorption of oxidized ABTS (1 mM) at 420 nm ($\varepsilon = 36 \times 10^{-3}$ M^{-1} cm^{-1}) at 25 °C (pH 3.5 for LCC3 and 4.5 for LcTv). One unit of enzymatic activity was defined as the amount of enzyme transforming 1 µmol of ABTS per min at the indicated pH and temperature [21].

2.6 Production and purification of recombinant LCC3 from *Trametes trogii*

Recombinant laccase LCC3 from *Trametes trogii* was produced in yeast *Pichia pastoris* and purified by Ni–NTA affinity chromatography as previously described [18]. Purified LCC3 activity was determined by ABTS oxidation (14,682 UE/L, pH 3.5, 25 °C) and total protein concentration (0.33 mg/mL) was measured following the Bradford method, using bovine serum albumin (BSA) as protein standard [22].

2.7 Laccases immobilization

The optimization of the immobilization conditions is discussed in the Electronic Supplementary Data file. For LCC3 immobilization, the corresponding solid was suspended in McIlvane´s Buffer at pH 7 and sonicated at 40 kHz for 5 min. The proper volume of the enzyme stock solution was added to reach the desired mass of protein per mass of support. The mixture was stirred at 350 rpm using an orbital shaker at 25 °C. For the analysis, the solid was separated by centrifugation at 3000 rpm for 5 min. The immobilized laccase was estimated as the difference between the total units incubated with the solid (initial) and the free enzyme quantified in the supernatant (final) using ABTS oxidation assay. The mass of enzyme was interpolated from an external calibration curve UE/L *vs.* mg/L.

2.8 Crystal violet (CV) bleaching

The bleaching experiments using the free enzyme were performed by adding 8µL (0.0026 mg) of the purified LCC3 extract to a CV solution (10 mg/L) prepared at the desired pH value. For the immobilized LCC3, the solid (2 mg) was suspended in the desired buffer using a vortex mixer for 2 min. Then, the proper aliquot of CV solution was added to reach an initial concentration of 10 mg/L. The mixtures were incubated a 350 rpm for 24 h at a given temperature. Finally, the samples were centrifuged at 3000 rpm during 2 min (for biocatalyst recovery) and the bleaching of the solution was determined by monitoring CV absorbance at 590 nm using an Ocean Optics modular spectrophotometer. The following equation was used to estimate the bleaching percentage:

$$CV\ bleaching\ (\%) = \frac{(Abs_0 - Abs_t) * 100}{Abs_t^{CV}} \quad (1)$$

Here, Abs_o and Abs_t correspond to CV absorbance in the solution at 590 nm at initial time and at a given time, respectively. Abs_t^{CV} represent the CV absorbance in a parallel blank test without enzyme at the given time "t".

The pH profile was obtained using Mc Ilvane's buffers (pH 2.6, 4.6, 6, 7 or 8) by incubation at room temperature (25 °C) during 60 min. The temperature profiles were measured incubating the mixtures at 25, 40, 50, 60 or 80 °C in the optimum pH value. To evaluate CV adsorption at each support (without immobilized laccase), the solid was suspended in buffer at pH 4.6 and mixed as described before. Then, it was added the proper CV aliquot to reach an initial concentration of 10 mg/L. These suspensions were stirred at 25 °C during 24 h under darkness.

The stability of the immobilized LCC3 was evaluated incubating each solid in buffer solution at pH = 6 for 24 h

under stirring at 350 rpm, after this time the solid was centrifuged and the filtered solution was used to evaluate the protein leaching using the ABTS assay. The solid was suspended in buffer solution, the CV aliquot was added, and the bleaching (%) was determined as before. Reuse and storage were tested in nine reaction cycles of 24 h, intercalated by two storage conditions. After each cycle, the solid was centrifuged, and new CV solution at the optimum pH was added, the system was brought to incubation at the optimum temperature for a next reaction cycle. The reaction cycles one to three were conducted with the fresh biocatalyst. The first storage condition was performed at 4 °C for 1 week (the solid was suspended in buffer pH = 7). After this period, the solid was tested in the reaction cycles four to six. Later, the recovered material was subjected to a second storage condition of 1 week at −15 °C. After this period the reaction cycles seven to nine were conducted as described before. The effect of the redox mediator, acetosyringone (ASG), was tested at 25 °C and pH 4.6 (optimal for free LCC3). For this, the proper amount of ASG to achieve a molar ratio of CV: ASG = 1: 4 was added just before CV.

3 Results and discussion

3.1 Host *w*-SiO_2 spheres

w-SiO_2 particles exhibit a complex structure with pore size distribution dependent on the functionalization of the silica surface. From TEM and SEM images in Fig. 1a, b, naked *w*-SiO_2 particles resulting from the synthesis (~550 nm diameter) can be described as a ~350 nm denser core surrounded by a ~200 nm radial lamellar zone that defines a wrinkled surface with walls width of ~10 nm. The N_2 adsorption–desorption isotherm for these particles (Fig. 2a) corresponds to a Type IV isotherm with an H3 hysteresis loop, characteristic of mesoporous systems [23]. The additional N_2 uptake at high P/Po is associated with non-rigid aggregates of plate-like particles, corresponding to the lamellar zone [24]. Naked *w*-SiO_2 exhibit a high surface area (520 m^2/g) and a bimodal distribution of pore diameters, as derived from BJH model (Fig. 2b), it shows a narrow distribution centered at 3.5 nm and a broad one above 5 nm. The narrow distribution corresponds to those pores formed by the CTAB template in the walls, while the wider distribution above

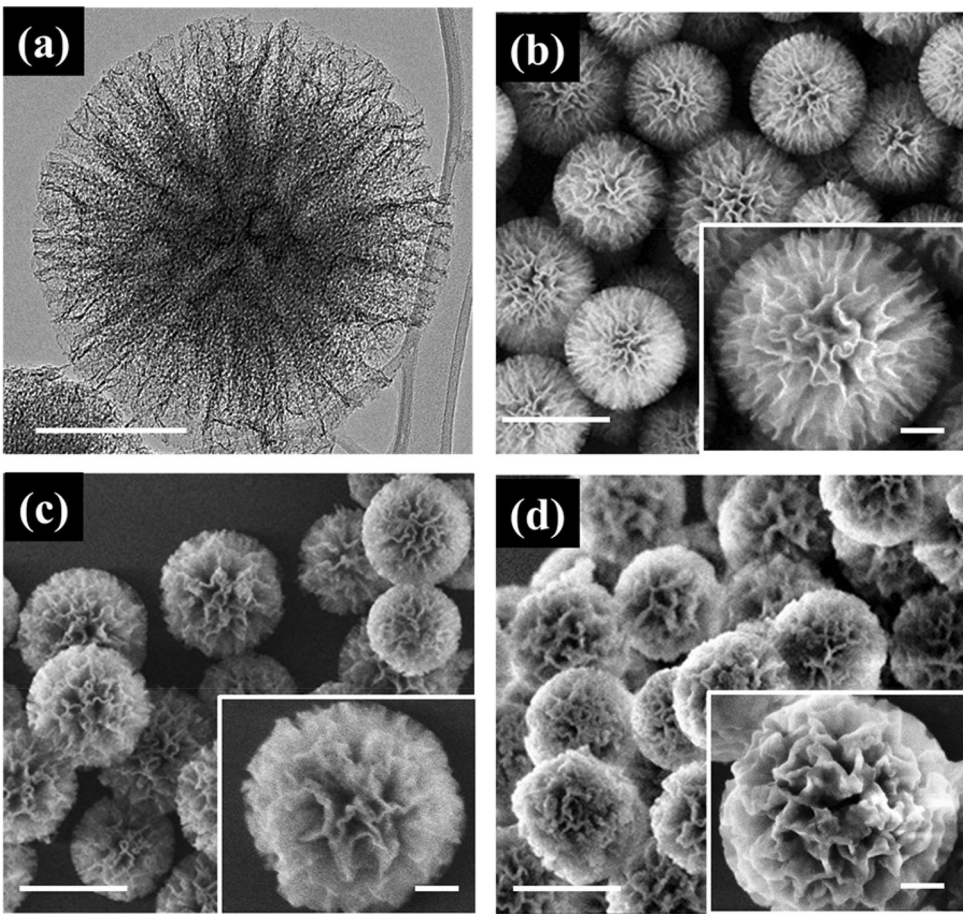

Fig. 1 **a** TEM image for *w*-SiO_2, (b-d) SEM images of *w*-SiO_2 spheres: **b** *w*-SiO_2, **c** *w*-SiO_2-NH_2 and **d** *w*-SiO_2-NH_2-GA. For the TEM image, the scale bar is 200 nm. The scale bar in the SEM images corresponds to 500 nm and for the insets, is 100 nm

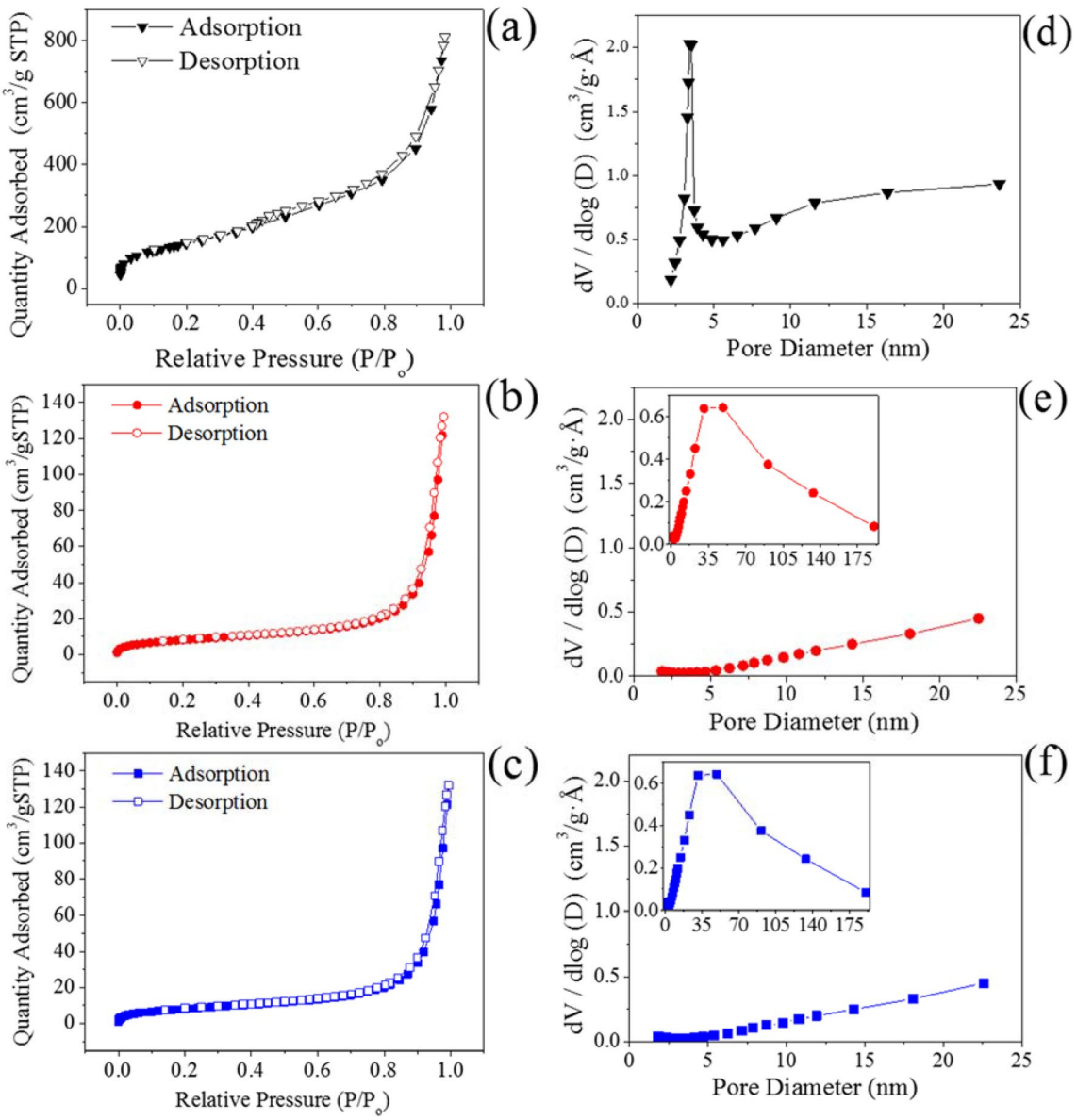

Fig. 2 N_2 adsorption–desorption isotherms (**a**, **b**, **c**) and pores size distribution calculated with BJH model (**d**, **e**, **f**) for the spheres: *w*-SiO_2 (**a**, **d**), *w*-SiO_2-NH_2 (**b**, **e**) and *w*-SiO_2-NH_2-GA (**c**, **e**)

5 nm is a consequence of the cavities formed between the corrugated porous walls [25].

Functionalization with APTES and APTES-GA leads to broadener walls (Figs. 1c, d) indicating that both are incorporated to the SiO_2 surface. This broadening is a consequence of silica dissolution and re-growth under the reaction conditions that is more likely when the silica network is not previously straightened by calcination. Here, calcination was disregarded in order to maintain a high density of hydroxyl surface groups [26, 27]. The functionalized spheres show type II isotherms typical in nonporous or macroporous materials, with a significant drop of the surface area and a slight increase of the particle's mean diameter, as shown in Table 1. Both functionalizing agents block the 3.5 nm pores with less impact on the bigger pores, indicating that APTES is anchored to the walls, and the cross-linking by GA in adjacent walls is negligible (insets in Fig. 2e, f) thus ensuring enough space to lodge the protein molecules that will interact with the functionalizing agents grafted in the wrinkled walls.

From elemental analysis (C, H, N), the nitrogen grafting is 1.8 mmol/g (2.5 wt.%) and, from the mass loss in TGA (shown in Figure S1) the imine formation is nearly complete after GA incorporation. The results from these experiments are compiled in Table 1. The presence of specific

Table 1 Particles mean diameter (Φ), specific surface area, pore volume, elemental analysis and weight loss of the functionalized particles in comparison to naked *w*-SiO_2

Solid	Φ* (nm)	SSA# (m^2/g)	Pore volume (cm^3/g)	C (%)	H	N	Weight loss& (%)
w-SiO_2	549	520	0.87	1.0	1.4	ND	4
w-SiO_2-NH_2	549	125	0.59	13.1	1.4	2.5	11
w-SiO_2-NH_2-GA	560	99	0.56	15.0	1.6	1.8	18

ND not detected

*=Particle mean diameter. It was measured from at least 50 particles using a 100KX SEM image; the standard deviation is ± 7%

#SSA = specific surface area

&The weight loss was measured in the (200–800) °C range for naked *w*-SiO_2 corresponding to the loss of silanol (Si–OH) groups and, in the (300–800) °C range for the functionalized *w*-SiO_2 spheres

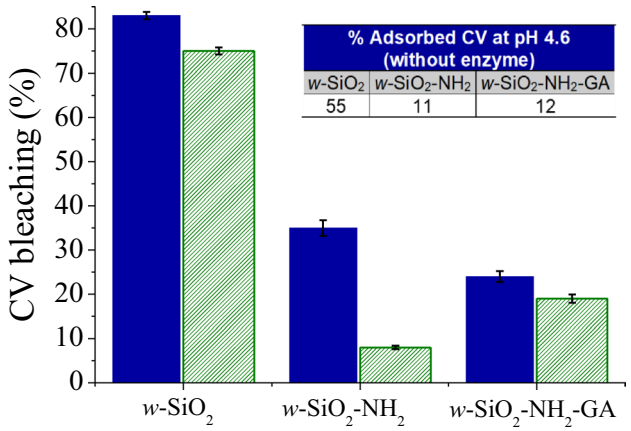

Fig. 3 CV bleaching at pH 4.6, 25 °C, and 24 h (optimal conditions for free LCC3). Columns with full filling represent the bleaching using fresh catalysts, columns with dashed filling represent the bleaching after incubation. CV = 0.02 mg (10 mg/L), LCC3: 0.0019 mg (0.04U) in *w*-SiO_2; 0.0033 mg (0.07U) in *w*-SiO_2-NH_2; and 0.0027 mg (0.06U) in *w*-SiO_2-NH_2-GA

surface groups, such as silanol groups, NH_2, C = O, imine bond was confirmed by FTIR (Figure S2).

3.2 Effect of the support on CV bleaching

An optimal solid biocatalyst sould be reusable with a retained enzymatic activity. The interaction with the support determines not only the loading but also the activity. The LCC3 performance was evaluated before and after a 24 h incubation in buffer solution to determine the effect of each support in the activity and stability. The CV bleaching (%) before incubation (full-filled columns) and after incubation (dashed columns) are shown in Fig. 3. The enzyme immobilized in naked *w*-SiO_2 exhibits the highest CV bleaching in both cases. However, an adsorption test (without enzyme) revealed that CV is greatly adsorbed on this support, as shown in the table inset. Whereas, in the functionalized materials the adsorption is low at the reaction pH. As the enzyme is just physically immobilized in *w*-SiO_2, it readily desorbs liberating surface sites for CV adsorption. This result indicates that using the naked *w*-SiO_2 particles, the CV removal is produced mainly by means of pollutant adsorption instead of the enzyme-mediated oxidation. The LCC3 performance depends both on the attached functional group and incubation in the reaction buffer. For fresh catalysts, *w*-SiO_2-NH_2 shows a higher CV bleaching than *w*-SiO_2-NH_2-GA. But the bleaching decreases in 72% for *w*-SiO_2-NH_2 after incubation. Therefore, *w*-SiO_2-NH_2-GA is much better to retain the enzyme activity. Based on these observations and considering the effect of each support on the immobilization yield (see discussion in ESI file), it can be highlighted that the *w*-SiO_2-NH_2-GA spheres, allows high enzyme loadings, ensures the stability of the immobilized LCC3 and shows a negligible interfere with the bleaching process, such as the described for naked *w*-SiO_2.

3.3 Performance of LCC3 immobilized on *w*-SiO_2-NH_2-GA

Figure 4 presents the pH and temperature effect on CV bleaching using LCC3 immobilized on *w*-SiO_2-NH_2-GA. The optimal pH shifts to a higher value in comparison to the free enzyme (Fig. 4a). It is known, that the general mechanism for laccases mediated-oxidation is highly affected by pH, as the electron transfer between the different copper (Cu) sites is hindered by interaction with hydroxyl species (OH^-) [28]. However, in porous SiO_2, the H_3O^+/ OH^- distribution inside the pores is different than in bulk solution, changing the enzyme microenvironment at higher pH [29]. This stabilization at circumneutral pH is an advantage because it prevents the need of an acidification step before oxidation. The incubation temperature has a smaller effect on free LCC3; the highest bleaching occurs at 50 °C, and is > 80% above this value. On the other hand, for the immobilized enzyme the optimal temperature is 40 °C and, after this value the activity decays up to 40%, probably related

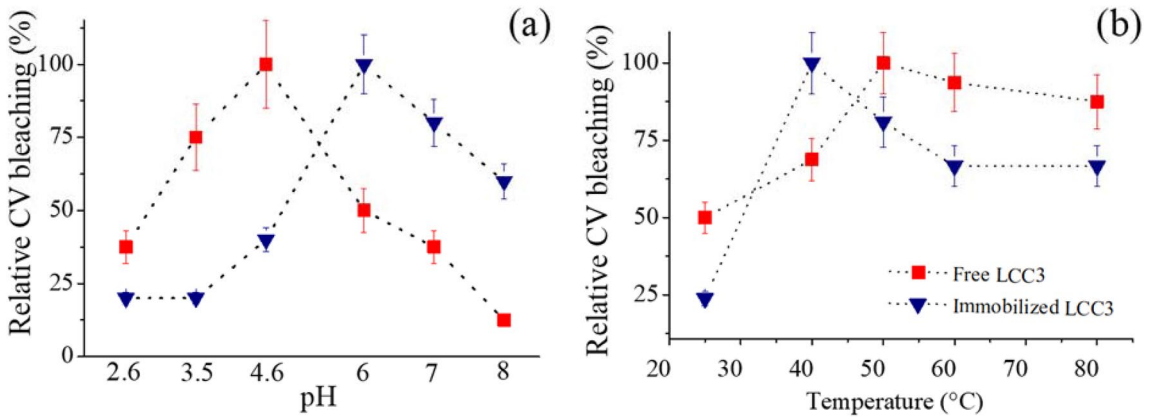

Fig. 4 Relative CV bleaching using free and immobilized LCC3 **a** pH profile (25 °C), **b** temperature profile (pH = 4.6 for free LCC3 and pH = 6 for immobilized LCC3). In all cases: t = 60 min, [CV] = 0.02 mg (10 mg/L), 0.0026 mg of free LCC3 (0.06U) or 2 mg of support containing 1.35 mg/g of LCC3 (0.06U)

to conformational changes in the immobilized molecules induced by temperature.

The reutilization for the immobilized LCC3, was tested up to nine reaction cycles at the optimal condition (pH = 6, 40 °C). Two storage periods were included between cycles three and six to demonstrate the robustness of the biocatalyst. According to Fig. 5a, for the first six reaction cycles, the relative CV bleaching did not change even after the storage at 4 °C for 1 week. On the other hand, when the solid was kept at -15 °C (1 week, pH = 7) the relative bleaching drops about 40%, but no changes are observed in the activity in subsequent reaction cycles (Fig. 5b). The activity drop is probably due to changes in the conformation of the enzyme during the freezing/de-freezing process. It is worth nothing that a significant feature of this system is the easy separation from the aqueous media because of the dimensions of the particles (diameter ~500 nm) which facilitates their separation and therefore storage to perform several reaction cycles with retention of the activity.

Finally, the enhancement of the enzymatic activity was studied with acetosyringone (ASG), an efficient redox mediator in the oxidation of several dyes using LCC3 [18]. The effect of this mediator on CV bleaching is shown in Fig. 6, compared to the free enzyme. The presence of ASG improves the CV bleaching in both cases, reaching more than 95% of transformation at 24 h. The similar kinetic profile comparing free and immobilized LCC3 suggest that immobilization does not alter the mechanism mediated by the ASG. It is noteworthy to point out that the effect of this redox mediator is lower at the optimal pH for the immobilized enzyme (pH = 6), and in this case the bleaching reaches 42% after 24 h (not shown). This redox mediator works poorly at higher pH as the redox potential for phenols decreases with pH [30]. Although new mediators could

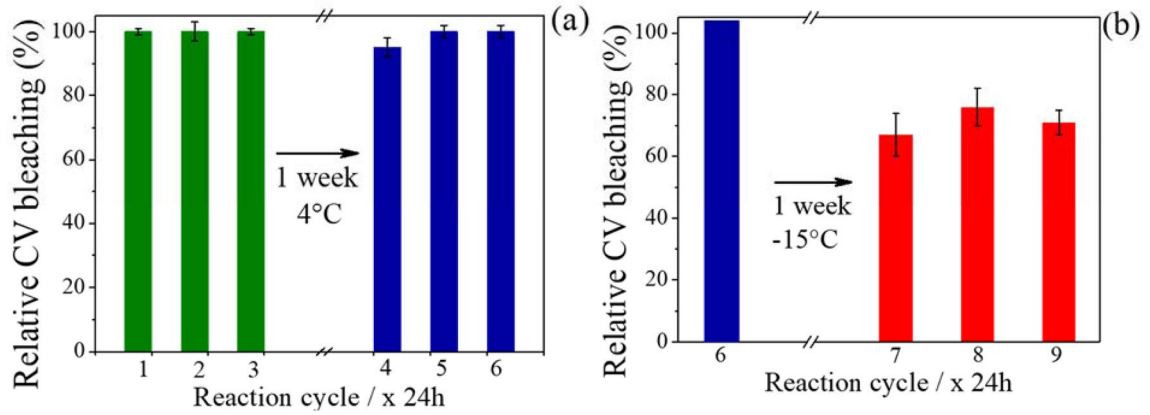

Fig. 5 Relative CV bleaching after several cycles of reuse and storage. **a** Reuse after storage at 4 °C for 1 week, relative bleaching is calculated by comparison with the first reaction cycle (using the fresh catalyst). **b** Reuse after storage at −15 °C for 1 week, relative bleaching is calculated by comparison with the sixth reaction cycle. Bleaching conditions: pH = 6, T = 40 °C, t = 24 h

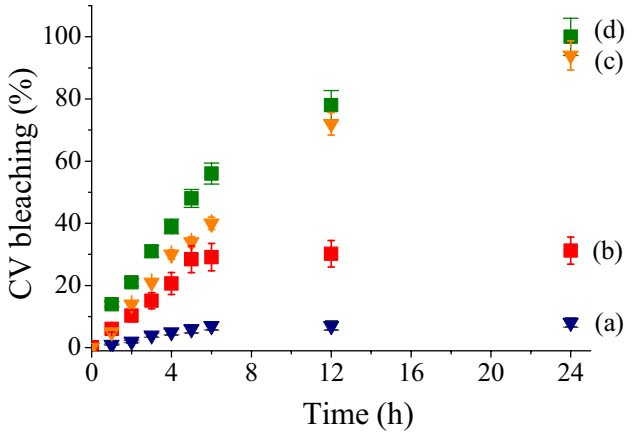

Fig. 6 Effect of acetosyringone (ASG) on CV bleaching at 25 °C and pH 4.6. **a** Immobilized LCC3, **b** free LCC3, **c** immobilized LCC3 + ASG, **d** free LCC3 + ASG. The ASG: CV molar ratio is 4:1. In all cases: [CV] = 10 mg/L (0.02 mg), 0.0026 mg (0.06U) of free enzyme and 2 mg of support containing 1.35 mg/g (0.06U)

enhance bleaching at the optimal pH of the immobilized enzyme, this will be addressed in a future research, as using redox mediators with the immobilized enzyme opens the door to extend the oxidizable substrates range for several applications.

4 Conclusions

The functionalized hierarchical meso/ macroporous silica spheres are remarkable supports for laccases immobilization. The morphology of these particles allows the grafting of APTES and GA in the wrinkled walls, while the large entries of the pores facilitate the accommodation of the enzyme without clogging of the porous system. This configuration yields a higher mass of immobilized enzyme per surface area, as compared to conventional mesoporous silica. The strategy developed here for LCC3 immobilization can be extrapolated to the other enzymes with biotechnological interest, as it gives a catalyst with high enzymatic activity at pH = 6, easy recovery and reuse which enables the use of redox mediators to boost the enzyme performance.

Acknowledgements KMF and LLCO acknowledge CONICET for the postdoctoral and doctoral scholarships, respectively. The authors are grateful to Maria Claudia Marchi (CONICET researcher) for the SEM images, Xavier Cattoen and Stephanie Kodjikian (Institut NÉEL, Grenoble) for the TEM images, Adriana Garcia and Vicente Povse (INQUIMAE) for the support during FTIR, TGA and microanalysis and, Ph.D. Verónica Lombardo (Centro Atómico Constituyentes, CNEA) for ASE and porosity measurments. SW and SAB are members of CONICET.

Funding This work was financed by: PICT-2013–1451, UBACyT 20020170200298BA and CONICET- PIP_11220170100289CO.

References

1. N. Thananukul, A. Phongphut, S. Prichanont, C. Thanachayanont, S. Fearn, B. Chayasombat, A comparative study on mesocellular foam silica with different template removal methods and their effects on enzyme immobilization. J. Porous Mater. **26**, 1059–1068 (2019). https://doi.org/10.1007/s10934-018-0705-1
2. Y.-C. Yang, J.R. Deka, C.-E. Wu, C.-H. Tsai, D. Saikia, H.-M. Kao, Cage like ordered carboxylic acid functionalized mesoporous silica with enlarged pores for enzyme adsorption. J. Mater. Sci. **52**, 6322–6340 (2017). https://doi.org/10.1007/s10853-017-0864-5
3. K. Hisamatsu, T. Shiomi, S. Matsuura, T.Y. Nara, T. Tsunoda, F. Mizukami, K. Sakaguchi, α-Amylase immobilization capacities of mesoporous silicas with different morphologies and surface properties. J. Porous Mater. **19**, 95–102 (2012). https://doi.org/10.1007/s10934-011-9452-2
4. J.M. Gómez, M.D. Romero, T.M. Fernández, S. García, Immobilization and enzymatic activity of β-glucosidase on mesoporous SBA-15 silica. J. Porous Mater. **17**, 657–662 (2010). https://doi.org/10.1007/s10934-009-9335-y
5. A. Dwevedi, Enzyme Immobilization, Springer International Publishing. Cham (2016). https://doi.org/10.1007/978-3-319-41418-8
6. D. Jung, C. Streb, M. Hartmann, Covalent anchoring of chloroperoxidase and glucose oxidase on the mesoporous molecular sieve SBA-15. Int. J. Mol. Sci. **11**, 762–778 (2010). https://doi.org/10.3390/ijms11020762
7. A.S. Maria Chong, X.S. Zhao, Functionalization of SBA-15 with APTES and characterization of functionalized materials. J. Phys. Chem. B. **107**(46), 12650–12657 (2003). https://doi.org/10.1021/jp035877+
8. K. Piontek, M. Antorini, T. Choinowski, Crystal structure of a laccase from the fungus trametes versicolor at 190-Å resolution containing a full complement of coppers. J. Biol. Chem. **277**(40), 37663–37669 (2002). https://doi.org/10.1074/jbc.M204571200
9. J. Li, L.-S. Li, L. Xu, Hierarchically macro/mesoporous silica sphere: a high efficient carrier for enzyme immobilization. Microporous Mesoporous Mater. **231**, 147–153 (2016). https://doi.org/10.1016/J.MICROMESO.2016.05.028
10. J. Pang, G. Zhou, R. Liu, T. Li, Esterification of oleic acid with methanol by immobilized lipase on wrinkled silica nanoparticles with highly ordered, radially oriented mesochannels. Mater. Sci. Eng. C. **59**, 35–42 (2016). https://doi.org/10.1016/j.msec.2015.09.088
11. V. Califano, F. Sannino, A. Costantini, J. Avossa, S. Cimino, A. Aronne, Wrinkled silica nanoparticles: efficient matrix for β-Glucosidase immobilization. J. Phys. Chem. C. **122**, 8373–8379 (2018). https://doi.org/10.1021/acs.jpcc.8b00652
12. D. Singh, N. Gupta, Microbial Laccase: a robust enzyme and its industrial applications. Biologia (Bratisl). (2020). https://doi.org/10.2478/s11756-019-00414-9
13. M. Deska, B. Kończak, Immobilized fungal laccase as "green catalyst" for the decolourization process – State of the art. Process Biochem. **84**, 112–123 (2019). https://doi.org/10.1016/j.procbio.2019.05.024
14. P. Baldrian, Fungal laccases – occurrence and properties. FEMS Microbiol. Rev. **30**, 215–242 (2006). https://doi.org/10.1111/j.1574-4976.2005.00010.x
15. J. Polaina, A.P. MacCabe (eds.), *Industrial Enzymes* (Springer, Netherlands, Dordrecht, 2007)
16. A. Piscitelli, C. Pezzella, P. Giardina, V. Faraco, G. Sannia, Heterologous laccase production and its role in industrial applications. Bioeng. Bugs. **1**, 254–264 (2010). https://doi.org/10.4161/bbug.1.4.11438

17. C.G. Daughton, Non-regulated water contaminants: emerging research. Environ. Impact Assess. Rev. **24**, 711–732 (2004). https://doi.org/10.1016/j.eiar.2004.06.003
18. P.A. Campos, L.N. Levin, S.A. Wirth, Heterologous production, characterization and dye decolorization ability of a novel thermostable laccase isoenzyme from trametes trogii BAFC 463. Process Biochem. **51**, 895–903 (2016). https://doi.org/10.1016/j.procbio.2016.03.015
19. I. Borón, S. Wirth, F. Battaglini, Versatile electrochemical platform for the determination of phenol-like compounds based on laccases from different origins. Electroanalysis **29**, 616–621 (2017). https://doi.org/10.1002/elan.201600470
20. D.-S. Moon, J.-K. Lee, Tunable synthesis of hierarchical mesoporous silica nanoparticles with radial wrinkle structure. Langmuir **28**, 12341–12347 (2012). https://doi.org/10.1021/la302145j
21. R. Bourbonnais, M.G. Paice, I.D. Reid, P. Lanthier, M. Yaguchi, Lignin oxidation by laccaseisozymes from trametesversicolor and role of the mediator 2,2'-azinobis(3-ethylbenzthiazoline-6-sulfonate) in kraft lignin depolymerization. Appl. Environ. Microbiol. **61**(5), 1876–1880 (1995)
22. M.M. Bradford, A rapid and sensitive method for the quantitation of microgram quantities of protein utilizing the principle of protein-dye binding. Anal. Biochem. **72**, 248–254 (1976). https://doi.org/10.1016/0003-2697(76)90527-3
23. Z. ALOthman, A Review: Fundamental Aspects of Silicate Mesoporous Materials. Materials (Basel). **5**(12), 2874–2902 (2012). https://doi.org/10.3390/ma5122874
24. D.-S. Moon, J.-K. Lee, Formation of wrinkled silica mesostructures based on the phase behavior of pseudoternary systems. Langmuir **30**, 15574–15580 (2014). https://doi.org/10.1021/la504207k
25. K. M. Fuentes, M. Sánchez-Dominguez, S. A. Bilmes, (2019) TiO 2 Nanoparticles Supported on Hierarchical Meso/Macroporous SiO2 Spheres for Photocatalytic Applications, Concepts Semicond. Photocatal, IntechOpen
26. P.M. Dove, N. Han, A.F. Wallace, J.J. De Yoreo, Kinetics of amorphous silica dissolution and the paradox of the silica polymorphs. Proc. Natl. Acad. Sci. **105**, 9903–9908 (2008). https://doi.org/10.1073/pnas.0803798105
27. R. Mueller, H.K. Kammler, K. Wegner, S.E. Pratsinis, OH surface density of SiO 2 and TiO 2 by thermogravimetric analysis. Langmuir **19**, 160–165 (2003). https://doi.org/10.1021/la025785w
28. K. Agrawal, V. Chaturvedi, P. Verma, Fungal laccase discovered but yet undiscovered. Bioresour. Bioprocess. **5**, 4 (2018). https://doi.org/10.1186/s40643-018-0190-z
29. S.Z. Mazlan, S.A. Hanifah, Effects of temperature and pH on immobilized laccase activity in conjugated methacrylate-acrylate microspheres. Int. J. Polym. Sci. **2017**, 1–8 (2017). https://doi.org/10.1155/2017/5657271
30. F. Xu, Oxidation of phenols, anilines, and benzenethiols by fungal laccases: correlation between activity and redox potentials as well as halide inhibition. Biochemistry **35**, 7608–7614 (1996). https://doi.org/10.1021/bi952971a